Assimilation of Passive Microwave Streamflow Signals for Improving Flood Forecasting: A First Study in Cubango River Basin, Africa

Yu Zhang, Yang Hong, XuGuang Wang, Jonathan J. Gourley, JiDong Gao, Humberto J. Vergara, and Bin Yong

***Abstract*—Floods are among the most frequently occurring and disastrous natural hazards in the world. The overarching goal of this study is to investigate the utility of passive microwave AMSR-E signal and TRMM based precipitation estimates in improving flood prediction at the sparsely gauged Cubango River Basin, Africa. This is accomplished by coupling a widely used conceptual rainfall-runoff hydrological model with Ensemble Square Root Filter (EnSRF) to account for uncertainty in both forcing data and model initial conditions. Three experiments were designed to quantify the contributions of the AMSR-E signal to the flood prediction accuracy, in comparison to the benchmark assimilation of in-situ streamflow observations, for both "Open Loop" and "Assimilation" modules. In general, the EnSRF assimilation of both in-situ observations and AMSR-E signal-converted-streamflow effectively improved streamflow modeling performance in terms of three statistical measures. In order to further investigate AMSR-E signals' contribution to extreme events prediction skill, the upper 10th percentile daily streamflow was taken as the threshold. Results show significantly improved skill and detectability of floods as well as reduced false alarm rates. Given the global availability of satellite-based precipitation from current TRMM and future GPM, together with soil moisture information from the current AMSR-E and future SMAP mission at near real-time, this "first attempt" study at a sparsely gauged African basin shows that opportunities exist for an integrated application of a suite of satellite data in improving flood forecasting worldwide by careful fusion of remote sensing and in-situ observations.**

***Index Terms*—AMSR-E, EnSRF, flood prediction, TRMM.**

Manuscript received August 21, 2012; revised November 24, 2012; accepted February 27, 2013.

Y. Zhang, Y. Hong, and H. J. Vergara are with the School of Civil Engineering and Environmental Science, University of Oklahoma, Norman, OK 73019 USA. They are also with the Advanced Radar Research Center, University of Oklahoma, Norman, OK 73019 USA (e-mail: yanghong@ou.edu; http://hydro.ou.edu).

X. Wang is with the School of Meteorology, University of Oklahoma, Norman, OK 73019 USA, and also with the Center for Analysis and Prediction of Storms, University of Oklahoma, Norman, OK 73019 USA.

J. Gao is with the School of Meteorology, University of Oklahoma, Norman, OK 73019 USA, and also with the NOAA/National Severe Storms Laboratory, National Weather Center, Norman, OK 73072 USA.

J. J. Gourley is with the NOAA/National Severe Storms Laboratory, National Weather Center, Norman, OK 73072 USA.

B. Yong is with the State Key Laboratory of Hydrology, Water Resources and Hydraulic Engineering, Hohai University, NanJing, China.

Color versions of one or more of the figures in this paper are available online at http://ieeexplore.ieee.org.

I. Introduction

EVERY year there are hundreds and thousands of flood events around the world that cause significant human suffering, loss of life and property damage [1]–[3]. In a changing climate, it is reasonably anticipated that the flood risk will not decrease but become more severe and frequent, thus threatening more regions around the world [4]. Therefore, accurate and precise forecasting of floods plays an increasingly important role in early warning systems to protect life and property.

In order to provide early warnings of impending disasters, hydrological models are typically applied for flood detection and prediction. The traditional way to improve the accuracy of streamflow simulation and prediction is to calibrate the model using manual or automatic approaches such as such as SLS (Stepwise Line Search) [5], SCE-UA (Shuffling Complex Evolution-University of Arizona) [6], and DREAM (DiffeRential Evolution Adaptive Metropolis) [7]. In addition to conventional calibration approaches, data assimilation can further improve the accuracy and precision of the modeling results by correcting the internal model states that are used as the initial condition of the forecast for the next time steps via assimilating available and reliable observations.

Ensemble data assimilation was first used in engineering and aerospace applications dating back to the 1960s. In recent decades, ensemble data assimilation has increasingly been expanded to many fields, especially meteorology, oceanography and hydrology. Data assimilation is defined as the insertion of reliable data into the dynamical model to improve the quality and accuracy of the estimates [8]. The Ensemble Kalman Filter (EnKF), which is a promising approach as it is robust and flexible in calculating background covariance [9], has broadly been applied in the research area of dynamic meteorology as well as numerical prediction [10]–[20]. Results show great potential of EnKF in enhancing modeling performance thus providing more reliable forecasts.

An increasing number of studies have been exploiting the potential to assimilate different types of hydrological observations by integrating EnKF with advanced hydrological models. One focus has been on the optimal use of soil moisture data with the EnKF (e.g., [21]–[26]). By assimilating soil moisture into an appropriately physically based model (either land surface model or hydrological model), better estimates of antecedent soil moisture condition result can be generated, thus enhancing the hydrologic prognostic capability of soil and streamflow states and

Digital Object Identifier 10.1109/JSTARS.2013.2251321

fluxes. However, the degree of improvement in forecast skill is contingent on the model structure and the quality of the observed data that are assimilated into the model. Chen *et al.* [26] pointed out that the failed attempt to improve streamflow prediction via assimilating soil moisture into the SWOT model was due to the deficiency of the model structure. A variety of studies have examined the applicability of assimilating streamflow observations into hydrological models in order to improve streamflow prediction and soil moisture conditions (e.g., [22], [27], [28]).

In addition to calibration and data assimilation techniques, the recent development of remote-sensing technology, which provides high temporal and spatial resolution forcing data such as precipitation and soil moisture, can greatly facilitate the improvement of flood forecasting [29]–[31]. However, it is recognized that the uncertainty with remote sensing data may cause additional errors to be propagated into hydrologic modeling results. For example, the TRMM (Tropical Rainfall Measurement Mission) – 3B42 RT forcing data used in this study, according to [32], [33], can lead to biased streamflow simulations through the error propagation from the model input to the model output in different basins. The commonly used batch calibration system for hydrologic analysis combines errors from input data and model structures into parameter uncertainties; sequential data assimilation has the potential to overcome this weakness by taking into account each source of uncertainty separately [34].

NASA AMSR-E (Advanced Microwave Scanning Radiometer for Earth observing system)/Aqua provides both soil moisture retrievals from the brightness temperature and the approximated river streamflow signals using the techniques proposed by Brakenridge *et al.* [31]. To date, however, previous assimilation studies with AMSR-E information are only focused on the soil moisture products but not on the remotely sensed streamflow signal. The overarching goal of this study is to investigate the potential utility of AMSR-E remotely-sensed signal data for hydrological model calibration and data assimilation in the Cubango River Basin, with rainfall forcing from TRMM-based satellite precipitation estimates. To do so, an ensemble square root filter (EnSRF), (also referred to as an EnKF without perturbing the observations) was applied and coupled with a widely tested rainfall-runoff hydrological model called HyMOD to overcome both the uncertainty of remotely sensed precipitation and streamflow data combined with the simplicity of the model structure.

To the best of our knowledge, this research is the first attempt to incorporate remotely-sensed streamflow, which was derived from the AMSR-E signals retrieved and provided by the Global Flood Detection System (GFDS, http://www.gdacs.org/flood-detection/), for hydrologic model parameter estimation and data assimilation. This study demonstrates the applicability of the globally-available AMSR-E signals and satellite-based precipitation estimates in enhancing the hydrologic performance via a combined calibration and data assimilation approach. It is shown that the assimilation of either gauge-observed or remote sensing-derived streamflow into the model updates all the internal model states (soil moisture content, quick and slow flow tank contents) with the expectation of thereby reducing the deviations between the model simulation and observation of streamflow. With the increasing availability of remote-sensing data over the globe (e.g., precipitation and soil moisture) and advances in computational power, it is possible that sequential data assimilation of remotely-sensed soil moisture and streamflow signals can be implemented in a real-time hydrological prediction system for improved hydrological forecasting, especially for the vast basins of the world that are only sparsely gauged.

Section II describes the Cubango river basin and the details of the model and data sources. Section III introduces the methodology of this study. In Section IV, the results of sensitivity analysis, calibration, data assimilation and threshold-based evaluation are discussed. Finally, a summary of results and conclusions are provided in Section V.

II. Study Region, Model and Data

A. Study Region

The Okavango River, which is the fourth longest river system in southern Africa, runs for about 1100 km from central Angola and flows through Namibia and Botswana (as shown in Fig. 1). The Okavango catchment is approximately 413,000 km^2, while the Okavango delta which lies downstream is about 15,000 km^2. Within the area of this catchment, Angola accounts for 48%, Nambia accounts for 37% and Botswana 15% of the land area. The Okavango river originates in the headwaters of central Angola, then the Cubango and Cuito tributaries meet to form the Cubango-Okavango River near the border of Angola and Namibia and flow into the Okavango Delta in Botswana. The upper stream region belongs to subtropical climate zone with annual precipitation around 1300 mm while the downstream region, which contains the Kalahari Desert, belongs to the semi-arid climate zone with annual precipitation around 450 mm [35], [36]. The headwater region, which is the northern part of the basin, is mainly covered by the ferralsols soil with a lower hydraulic conductivity. The headwater region also has a high forest cover and contributes significantly to the river runoff [36]. The rest of the basin is dominated by arenosals soil (www.sharing-water.net), which is very porous with high hydraulic conductivity, so that water drains rapidly, leaving little moisture for plants. As mentioned in [36], around 95% of inflow is lost in the atmosphere due to high potential evapotranspiration rate and only a small portion contributes to groundwater.

Several studies in the Okavango River Basin have investigated the hydrological response under climate change [36]–[40]. Since the Okavango River basin is one of the most important economic and water resources in southern Africa, additional studies have been solicited to assist in the decision-making for water management in this basin. The main tributary of Okavango River, the Cubango River, which is mainly located in Angola, is selected as the study basin. Fig. 1 shows the location of the Cubango River in southwest Africa, which accounts for a majority of the available water resources in the Okavango river. The Rundu gauge station is located at the outlet of Cubango River, a location where both the ground gauge-based streamflow observation and the remote-sensing discharge estimates (i.e., AMSR-E M/C ratio signal) are available.

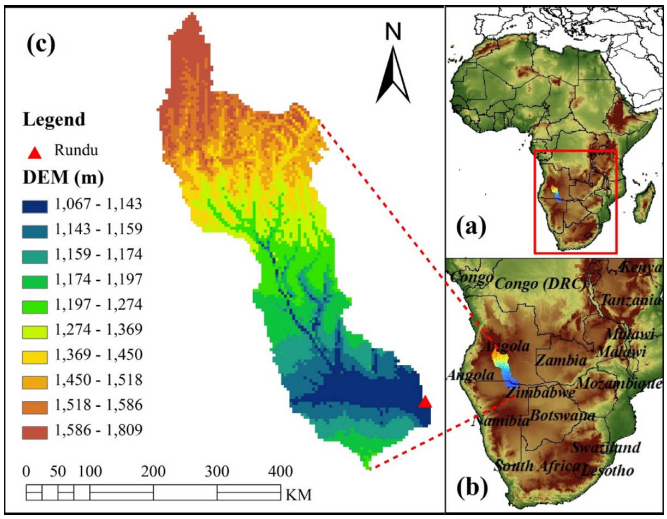

Fig. 1. Map of research region – Cubango River Basin, South Africa. (a) African; (b) Southern Part of Africa; (c) Cubango River.

TABLE I
PARAMETER RANGE OF HYMOD [43]

Parameter	Unit	Range
C_{max}	mm	1-500
b_{exp}	-	0.1-2
α	-	0-0.99
N_q	-	1-inf
R_q	day	0.1-0.99
R_s	day	0-0.1

B. Model

To concentrate on the effectiveness of the Ensemble Square Root Filter, the conceptually simple Hydrological MODel (HyMOD) described in [42] was utilized. This model commonly consists of several quick flow reservoirs and one single reservoir for slow flow; the quick flow reservoirs and the slow flow reservoir operate in parallel as routing components. The parameters of HyMOD and their reasonable ranges are as shown in Table I [42]: (1) $C_{\max}$: maximum storage capability in the catchment; (2) $b_{\exp}$: the degree of spatial variability of the soil moisture capacity within the catchment; (3) α: quick-slow split parameter; (4) N_q: number of quick flow routing tanks; (5) R_q: quick flow routing tanks rate parameter; and (6) R_s : slow flow routing tanks rate parameter. The internal states are (1) $S(t)$: soil moisture accounting tank state contents; (2) X_q: quickflow routing tanks state contents with dimension of $1 * \mathrm{Nq}$; and (3) X_s: slowflow routing tank state contents. Following evaporation, the remaining rainfall is used to fill the soil moisture storage and then the excess rainfall splits into quickflow reservoir and slowflow reservoir by the quick-slow split parameter α. The flow in each reservoir is governed by quick flow routing tanks rate parameter R_q and slow flow routing tanks rate parameter R_s [43], [44]. In summary, the input variables should consist of the precipitation and the Potential Evapotranspiration PET, while the main output variable is the streamflow Q.

C. Data

With the development of remote-sensing techniques, the application to distributed hydrologic modeling especially in sparse or even ungauged basins has dramatically improved. Remote-sensing data with higher spatial and temporal resolution can provide information over the globe with less cost and less manual maintenance involved. These data can be used as the forcing data (e.g., precipitation, potential evapotranspiration) to drive the hydrologic models and to calibrate the parameters as well, thus enabling the flood forecasts and water resources management tools in most of the developing countries where conventional ground-based measurements are scarce. The Okavango River Basin is considered to be poorly gauged. Sparse ground gauge-based precipitation measurements are available in the Cubango sub-basin where most runoff is generated [45]. In this study, remotely-sensed precipitation and potential evapotranspiration are incorporated to drive the model while both the gauge measurement and the remotely-sensed estimation of streamflow are adopted to calibrate the model.

TRMM Multisatellite Precipitation Analysis (TMPA) provides two standard 3B42-level products: the near-real-time 3B42 RT which uses the TRMM combined instrument dataset to calibrate the data and the post-real-time research product 3B42 V7 (level 7) which adjusts the rainfall accumulation by gauge analysis [46]. Both 3B42 RT and 3B42 V6 products are quasi-global with coverage from 50°N to 50°S latitude. In this study, the TRMM 3B42 RT with the spatial resolution of 0.25° (approximate to 25 km in the tropical area) and temporal resolution of three hourly, is processed into daily accumulation as well as basin average and applied as the forcing data to drive the hydrological model. PET (potential evapotranspiration) comes from the Famine Early Warning System Network (FEWS NET; http://igskmncnwb015.cr.usgs.gov/Global/) with a spatial resolution of 0.25°, and is likewise processed into daily and basin average as additional forcing to the model.

For the benchmarks that were used to calibrate the model, both the ground gauge-observed streamflow from the local government and the AMSR-E signal converted streamflow were applied in this study. Dartmouth Flood Observatory (DFO, http://www.dartmouth.edu/~floods/), as well as GFDS, uses the AMSR-E sensor for discharge estimation in global scope for flood monitoring. Besides these two systems, other studies also explore the possibility of estimating the discharge based on the AMSR-E sensors [47]–[49]. This study uses the conventional Dartmouth algorithm [31], a polynomial model (refer to part 3.2), to retrieve the actual streamflow (in m^3/s) from the AMSR-E C/M radiance ratio.

III. METHODOLOGY

A. Streamflow Estimation From AMSR-E Signals

The GFDS uses the near real-time satellite-based, remote-sensing data to monitor floods over the globe. In this system, a passive microwave sensor, AMSR-E, together with TRMM TMI (TRMM Microwave Imager) sensor, are used to measure the brightness temperature at 36.5 GHz, descending orbit with horizontal polarization, which responds to surface wetness and

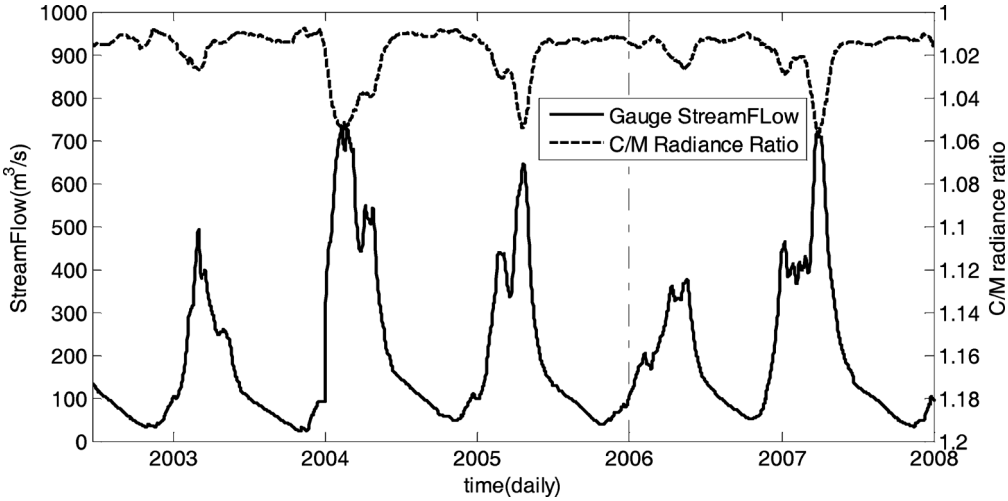

Fig. 2. Time series plot of C/M radiance ratio and observed streamflow from Jun-22-2002 to Dec 31-2007.

thus flooding [31]. It should be noted that though AMSR-E-polarized measures the brightness temperature (also expressed as radiance) both horizontally and vertically at 6 frequencies from 6.9 to 89.0 GHz, only 36.5 GHz at horizontal polarization is selected to measure the change of river discharge through a series of sensitivity tests [31]. A wet pixel (usually over the surface of a river) is selected to measure the brightness temperature of the measurement (M) area while an adjacent dry pixel is selected to measure the brightness temperature of the calibration (C) area (usually over the land near the wet pixel); the fraction of the measurement and calibration brightness temperature is referred as the M/C ratio signal ((1)).

$$\frac{M}{C}\ Ratio = \frac{Tb_m}{Tb_c}. \tag{1}$$

The M/C ratio signal data are provided by GFDS. Some details about selecting the M/C pixels should be noted: (1) The calibrated dry pixel C is located near the measurement wet pixel M so that changes such as vegetation, soil texture, etc. at those locations are more likely to be correlated. In other words, those two locations are more likely to share similar conditions (e.g., vegetation, and soil texture); (2) C and M are within a short distance so that the measurement acquired by AMSR-E are effectively contemporaneous; (3) M is selected to have the largest change in water surface area and relatively high sensitivity; (4) C is selected to be close to M but is located far enough to be not affected by flood inundation; (5) Moderate Resolution Imaging Spectroradiometer (MODIS) is applied to assist selecting M where flow area expansions occur [1], [31]. The main merit of the AMSR-E passive microwave sensor onboard the NASA EOS Aqua satellite is that it is not restricted by cloud cover and provides data availability for daily flood monitoring over the globe. In addition, since nighttime radiation is more stable than during the day, the descending (nightly) orbit with a footprint size of approximately 8×12 km is used. For additional details, refer to [1, Fig. 3.] which illustrates how the AMSR-E sensor can be used to detect flooding.

The C/M radiance ratio, which is the reciprocal of M/C ratio signal, is correlated at a significant level with observed streamflow as shown in Fig. 2. The relationship can also be visualized by the scatter plot shown in Fig. 3. Here, the observed streamflow is used to calibrate the orbital gauging measurements (the C/M radiance ratio signal) into in-situ discharge units (m^3/s) via a quadratic polynomial regression as shown in Fig. 3. Some other regressions were also tested in this study but not listed in this paper; it turns out the nonlinear quadratic polynomial regression outperformed the linear regression and other polynomial regressions. This arithmetic "pair ratio" (C/M radiance ratio as shown in (1)) approach proposed by Brakenridge, accounts for the inherent correlated changes between the brightness temperature ratio and river gauge data [31]. Brakenridge also demonstrated that AMSR-E data, calibrated via the paired measurement approach, and obtained over carefully selected river reaches, can characterize river discharge changes at a useful level of accuracy [31]. It should be noted that the parameters of the quadratic polynomial equation as shown in Fig. 3 are calibrated using both the gauge streamflow and AMSR-E signals data sets from 22 Jun 2002 to 31 Dec 2005. Following conversion, the correlation coefficient between the signal-converted streamflow and the observed streamflow is 0.95, the Bias is 1.91% and the RMSE (Root Mean Square Error) is 56.64 m^3/s during this period [note: capitalized "Bias" in this paper refers to the statistical index that is calculated by (17)].

The datasets from 1 Jan 2006 to 31 Dec 2007 are applied to validate the performance of this regression method. Fig. 4 indicates that the signal-converted streamflow is well correlated with gauge observations from 2002 to 2007, especially during the peak flow periods. However, overestimation of streamflow exists during the low flow period because the AMSR-E sensors are not sensitive to low flows. In addition, this approach is applied to medium- to large-sized basins. The accuracy of the AMSR-E signals for basins with less than 50000 km^2 drainage areas needs further investigation [50]. Additional factors influencing the utility of AMSR-E data for streamflow estimation include the width of the river, channel geometry, water temperature relative to land, and measurement pixel resolution.

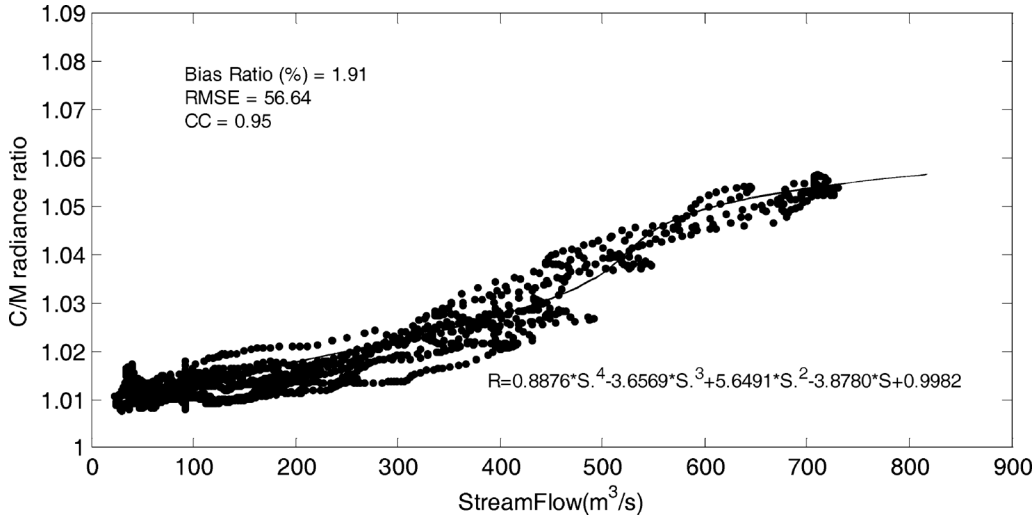

Fig. 3. Scatter plot and rating curve equation comparing daily $\mathrm{C/M}$ radiance ratio versus gauge based streamflows (In the equation, R refer to runoff /streamflow and S refer to signal).

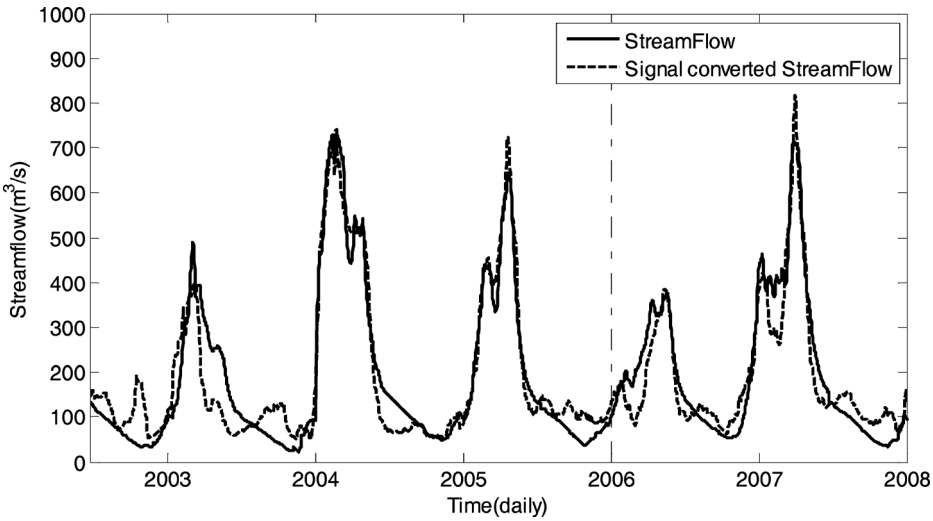

Fig. 4. Observed streamflow V.S. signal converted streamflow from Jun-22-2002 to Dec 31-2005.

B. Model Calibration and Validation

There are two general approaches for hydrologic model calibration: manual calibration and automatic calibration. The manual calibration approach, which is also expressed as "expert calibration", is largely based on the experience of the modeler. In contrast, the automatic calibration approach, which is largely dependent on the computational power and the efficiency of the algorithm, has been widely applied in hydrological calibration and it is often regarded as a quicker solution for arriving at a useful, calibrated model [41].

In this study, an automatic parameter estimation method called DREAM (Differential Evolution Adaptive Metropolis) developed by Vrugt [7], was applied to calibrate all the six parameters of HyMOD using gauge observations (in experiment 1&2 as described in Section III.D) and AMSR-E signal converted streamflow (in experiment 3 as described in Section III.D), respectively. DREAM, uses a sophisticated method to estimate the posterior probability density function in complex, high–dimensional sampling problems and resulted in a successful calibration of the HyMOD model parameters. From the authors' experience, the sensitivities of the parameters $\mathrm{C_{max}}$ which controls the quantity of excess rainfall and the routing parameter R_q which controls the residence time of quick-flow are relatively higher, then followed by α, $\mathrm{b_{exp}}$ and R_s . From the previous experiences [42]–[44], the number of quick-flow tanks N_q is somewhat sensitive but usually the recommended best value is three for small- to medium-sized basins.

The time series of the precipitation, PET, gauge streamflow observation, and AMSR-E signal are from 22 Jun 2002 (the starting date of the AMSR-E data) to 31 Dec 2007 due to the data availability. The calibration period spans 2003 to 2005, and the validation period is from 2006 to 2007. For each experiment, a warm-up period from 22 Jun 2002 to 31 Dec 2002 was run ahead of each experiment to initialize the internal model states.

C. Data Assimilation Approach: EnSRF

A sequential data assimilation technique called Ensemble Square Root Filter (EnSRF), which is also referred to as EnKF without perturbing observations, is applied to assimilate different streamflow observations into HyMOD. Compared to

the traditional EnKF which requires perturbing both forcing data and observations, for the EnSRF, only the forcing data is perturbed and the ensemble mean is updated by the observation. Whitaker and Hamill demonstrated that there is no additional computational cost by EnSRF relative to EnKF, and EnSRF performs more accurately than EnKF for the same ensemble size [51]. But it still remains a research topic to compare the accuracy and efficiency of different sequential data assimilation approaches (e.g., EnKF, EnSRF).

Let X^b be the background model forecast, which is also called the first guess in data assimilation ($n\times 1$ dimension and n is the number of emsembles); let y be the observation ($p\times 1$ dimension and p is the number of observations), which is the streamflow measurements in this study; let H be the observation operator that converts the states in the model into observation space ($p \times n$ dimension); the estimate of the analyzed state X^{a} can be described by the traditional Kalman filter update function [51] ($n\times 1$ *dimension*),

$$\mathrm{X}^{\mathrm{a}} = \mathrm{X}^b + \widehat{\mathrm{K}}(\mathrm{y} - \mathrm{H}(\mathrm{X}^b)). \tag{2}$$

In (2), $\widehat{\mathrm{K}}$ refers to the traditional Kalman gain. Let's denote the ensemble X^b as

$$X^b = (x_1^b, x_2^b, \ldots, x_n^b). \tag{3}$$

Where we ignore time index and the subscript represents the ensemble member. The ensemble mean is then defined as

$$\overline{X^b} = \frac{1}{n}\sum_{i=1}^{n} x_i^b. \tag{4}$$

The perturbation from the mean for the i th member is

$$x_i'^b = x_i^b - \overline{x^b}. \tag{5}$$

Then X'^b is defined as a matrix formed from the ensemble of perturbations:

$$X'^b = (x_1'^b, x_2'^b, \ldots, x_n'^b). \tag{6}$$

An estimation of background error covariance is defined as

$$\widehat{P}^b = \frac{1}{n-1} X'^b (X'^b)^{\mathrm{T}}. \tag{7}$$

However, in practice, we do not calculate $\widehat{P}^b$, but rather calculate $\widehat{\mathrm{P}}^b\mathrm{H}^{\mathrm{T}}$ and $\mathrm{H}\widehat{\mathrm{P}}^b\mathrm{H}^{\mathrm{T}}$ are evaluated by the following equations In order to estimate the Kalman gain $\widehat{\mathrm{K}}$ ::

$$\widehat{\mathrm{P}}^b\mathrm{H}^{\mathrm{T}} = \frac{1}{\mathrm{m}-1}\sum_{i=1}^{m}(\mathrm{X}_i^b - \overline{\mathrm{X}}^b)(\mathrm{H}(\mathrm{X}_i^b - \overline{\mathrm{H}(\mathrm{X}^b)}))^{\mathrm{T}} \tag{8}$$

$$\mathrm{H}\widehat{\mathrm{P}}^b\mathrm{H}^{\mathrm{T}} = \frac{1}{\mathrm{m}-1}\sum_{i=1}^{m}(\mathrm{H}(\mathrm{X}_i^b) - \mathrm{H}(\overline{\mathrm{X}}^b))(\mathrm{H}(\mathrm{X}_i^b - \overline{\mathrm{H}(\mathrm{X}^b)}))^{\mathrm{T}}. \tag{9}$$

Here, m is the ensemble size. Then the traditional Kalman gain $\widehat{\mathrm{K}}$ can be calculated by (10),

$$\widehat{\mathrm{K}} = \widehat{\mathrm{P}}^b\mathrm{H}^{\mathrm{T}}(\mathrm{H}\widehat{\mathrm{P}}^b\mathrm{H}^{\mathrm{T}} + \mathrm{R})^{-1}. \tag{10}$$

R is the observation error covariance with a dimension of $p\times p$. In EnSRF, the reduced Kalman gain $\widetilde{\mathrm{K}}$ is used to update the deviation from the ensemble mean as estimated by the following equation,

$$\widetilde{\mathrm{K}} = \left(1 + \sqrt{\frac{\mathrm{R}}{\mathrm{H}\widehat{\mathrm{P}}^b\mathrm{H}^{\mathrm{T}} + \mathrm{R}}}\right)^{-1} \widehat{\mathrm{K}}. \tag{11}$$

The ensemble mean can be updated by

$$\overline{\mathrm{X}}_i^{\mathrm{a}} = \overline{\mathrm{X}}_i^b + \widehat{\mathrm{K}}(\mathrm{y} - \mathrm{H}(\overline{\mathrm{X}}_i^b)). \tag{12}$$

The perturbation (deviation of ensemble mean) can be updated by

$$\mathrm{X}_i'^{\mathrm{a}} = \mathrm{X}_i'^b - \widetilde{\mathrm{K}}\mathrm{H}(\mathrm{X}_i'^b). \tag{13}$$

The final analysis follows as

$$\mathrm{X}_i^{\mathrm{a}} = \overline{\mathrm{X}}_i^{\mathrm{a}} + \mathrm{X}_i'^{\mathrm{a}}. \tag{14}$$

As mentioned above, when the EnSRF is applied, the forcing data (which is the precipitation in this study) needs to be perturbed. Precipitation perturbations in this study are defined as

$$\mathrm{P}_i = \mathrm{P} + \varepsilon_i \tag{15}$$

where ε_i is a random noise factor drawn from a Gaussian distribution

$$\varepsilon_i \sim \mathrm{N}(0, \mathrm{R}). \tag{16}$$

Since this study utilizes a lumped model HyMOD, the satellite-derived precipitation is aggregated into a basin average at every time step as the forcing input of the model, so no spatial error correlation is computed in the generation of the precipitation perturbation due to the feature of the lumped model. Regarding the temporal error correlations, the equation does not directly account for the temporal error correlations. At each time step, an independent rainfall error is generated by Gaussian distribution (refer to (15) and (16)) and added to the original basin average precipitation.

D. Experimental Design

The primary forcing datasets for the Cubango River basin come from the TRMM RT remote-sensing product and the potential evapotranspiration data from FEWS (http://igskmncnwb015.cr.usgs.gov/Global). Three experiments were performed for testing the efficiency of improving the streamflow simulations by assimilating different sources of observations. First, rainfall and runoff observations from June 2002 to December 2005 were used to calibrate the model parameters without data assimilation following the warm-up period. Then, both the gauge-based streamflow observation and the AMSR-E signal converted streamflow were assimilated separately into HyMOD to update all the internal states at each assimilation cycle, which is daily in this study for both calibration and validation period. The modeling results of these three experiments

TABLE II
INTRODUCTION OF EXPERIMENTS DESIGN.

Experiments	Calibration Benchmark	Data Assimilated into Model
Exp1	Ground Gauge Observed Streamflow	Ground Gauge Observed Streamflow
Exp2	Ground Gauge Observed Streamflow	AMSR-E M/C Ratio Signal Converted Streamflow
Exp3	AMSR-E M/C Ratio Signal converted streamflow	AMSR-E M/C Ratio Signal Converted Streamflow

are evaluated by the gauge-observed streamflow, which is always considered as the most accurate and reliable observation of streamflow.

In the first experiment, the model was calibrated by the gauge-observed streamflow and then the gauge observation was also assimilated into HyMOD to estimate the internal model states. This experiment is the benchmark for all experiments, which are summarized in Table II. In the second experiment, the model was similarly calibrated using the gauge-observed streamflow; however, in the assimilation step, the AMSR-E signal converted streamflow was incorporated into HyMOD in lieu of the gauge-observed streamflow data assimilated in experiment 1.

In the third experiment, the model was calibrated by the AMSR-E signal converted streamflow and then it was also assimilated into model to correct the model states for each assimilation cycle, without gauge-based observations involved.

E. Sensitivity Analysis

Research has been carried out in the sensitivity analysis among the spread of precipitation ensembles, observation error, ensemble size, and their impacts on data assimilation efficiency [27], [51]. Here, the "spread of the precipitation" is the white noise that is added into the precipitation to generate the precipitation ensembles. In other words, it is a measure of the difference between the precipitation ensemble members and is represented by the standard deviation (e.g., the parameter R is (11)). Pauwels *et al.* [27] analyzed the sensitivity of observation error; results show that the increase in the observation error leads to a decrease in the accuracy of the modeled discharge. Whitaker *et al.* [51] pointed out that with the enlargement of the ensemble size the modeled result improved up to a point where the modeled result remained the same. Those two studies mentioned above only analyzed the sensitivity of a single factor (e.g., observation error and ensemble size) affected in the effectiveness of data assimilation. Actually, the effectiveness of EnSRF, which can be evaluated by an NSCE (Nash-Sutcliffe Coefficient of Efficiency) statistic, should be a function of several factors (i.e., observation errors, spread of precipitation and ensemble size). In this study, a joint sensitivity analysis has been carried out to evaluate the mutual impacts of various observation errors, spread of precipitation and ensemble sizes for assimilating different sources of streamflow observations. Finally an optimal and reasonable point (with certain observation error, spread of precipitation and ensemble size) that yields the best simulation results when applying EnSRF will be identified and then utilized in the data assimilation experiments. It should be noted that the sensitivity analysis is applied after the model calibration step to avoid the bias in the model, and the sensitivity analysis is only applied for the calibration period.

F. Evaluation Metrics

In this study, three commonly used statistical indicators were used to assess the long time series model performance with and without the EnSRF data assimilation technique. Bias Ratio quantifies the difference between the simulated streamflow and the observed streamflow as described by the following equation:

$$Bias(\%) = \frac{\sum (y_i - x_i)}{\sum x_i} * 100. \tag{17}$$

In (12)–(14), x_i is the observed streamflow and y_i is the simulated streamflow. Normalized Root Mean Square Error is used to measure random errors as follows:

$$RMSE(\%) = \frac{\sqrt{\frac{\sum (x_i - y_i)^2}{n}}}{\overline{x}} * 100. \tag{18}$$

For both Bias and RMSE, the smaller their values are (i.e., closest to 0), the better the model result is. Small values of Bias and RMSE signify the modeling results are close to the corresponding observations in regards to systematic bias and random errors.

NSCE is a frequently used statistic to quantify the agreement between the model simulation and the ground observation. The perfect value of NSCE is 1. If the value of the NSCE is below 0, it indicates that the mean of the observation is a better predictor than the model.

$$NSCE = 1 - \frac{\sum (x_i - y_i)^2}{\sum (x_i - \overline{x})^2}. \tag{19}$$

In order to further evaluate the performance of EnSRF-coupled-HyMOD in flood detection during the peak flow period, a high flow threshold is defined as the top 10% daily streamflow quantile, and the categorical verification statistics of Probability of Detection (POD), False Alarm Ratio (FAR), Critical Success Index (CSI) and Equitable Threat Score (ETS) are used to evaluate the correspondence between the simulated and observed runoff above the high flow threshold. For specific descriptions of POD, FAR, CSI and ETS, please refer to Appendix.

IV. RESULTS

A. Sensitivity Analysis of the Ensemble Size, Observation Error and Spread of Precipitation

As shown by Fig. 5, observation errors of 5%, 8%, 10%, 13%, 15%, 18%, and 20%, spreads of precipitation of $0.10, 0.20, 0.30, \ldots 1.90$, and 2.00, and ensemble sizes of

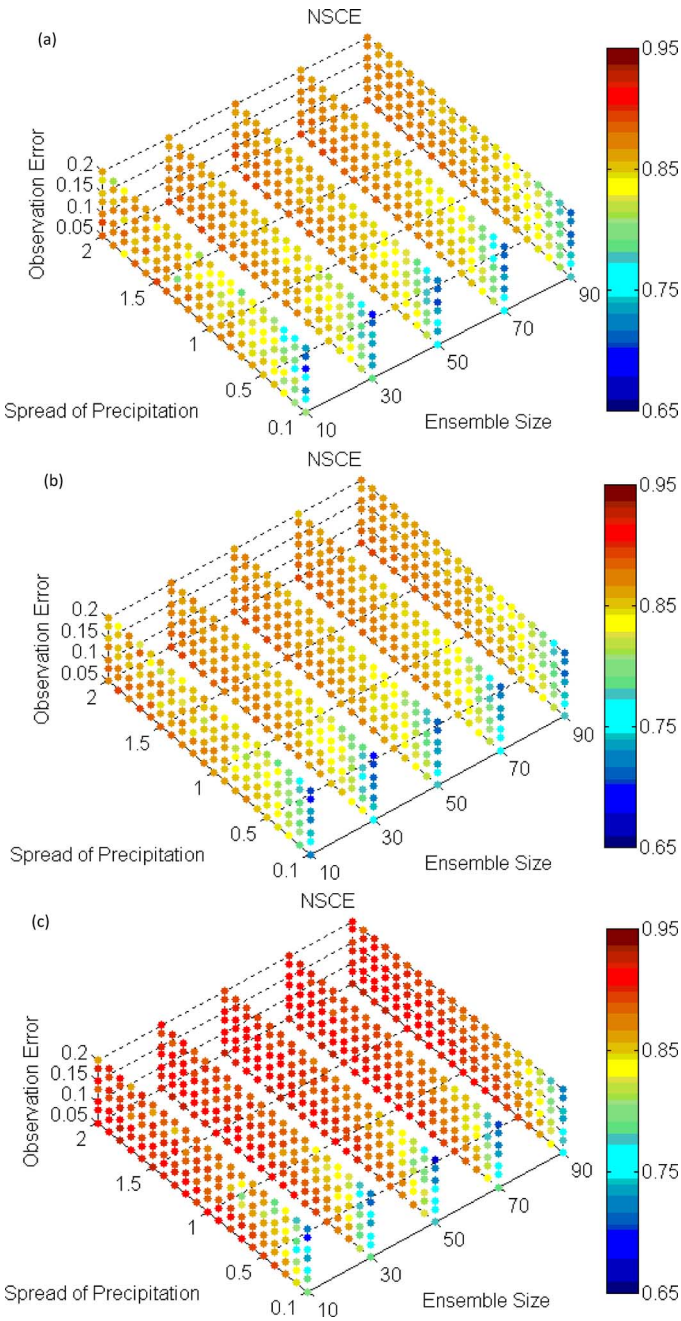

Fig. 5. Sensitivity analysis regarding observation error spread of precipitation, and ensemble size taking NSCE as the evaluation index. (a) Experiment 1; (b) Experiment 2; (c) Experiment 3.

10, 30, 50, 70, and 90 were tested to carry out the sensitivity analysis on the impact of assimilating different sources of streamflow observations to the improvement of modeled streamflow. In the sensitivity analysis for the three experiments, NSCE was taken as the evaluation metric.

Fig. 5(a), which shows the sensitivity analysis results for experiment 1, indicates increasing the observation error leads to a decrease in the accuracy of the modeled streamflow, which corresponds to the conclusion in [27]. From the sensitivity plot, it appears a value of 5% is an appropriate assumption describing the observation error. As the observation error goes up from 5% to 20%, the NSCE decreases (see from the vertical direction from Fig. 5(a)). It may go down below 5% for a better NSCE value, but actually the NSCE does not change much when observation error goes below 10%, which indicates the model performance is not sensitive when the observation error is smaller than 10%. In addition, based on previous experiences from USGS (U.S. Geological Survey), the error of streamflow that is from the gauge observation is usually around 8% [52] which is within the reasonable observation error range: 5%-10%. Due to the deficiencies within the simple structure of HyMOD, a larger background covariance was generated thus making the results much more dependent on the observation. In other words, during the assimilation procedure when the observation error is assumed to be smaller, the Kalman gain is increasing, which makes more corrections from the first guess to the observations. Based on the previous experience form USGS, in this case, for the time series assimilation experiment, 8% is assumed as the observation error for experiment 1 to produce the result in Fig. 6(a). Regarding the ensemble size, the NSCE increases when the ensemble size is enlarged from 10 to 50. However, when the ensemble size is further increased from 50 to 90, it does not lead to a further improvement in NSCE, which means the ensemble size of 50 members was large enough to produce the optimal modeling results. In addition, increasing the spread of precipitation also contributes to the improvement of the modeling result. By increasing the spread of precipitation from 10% to 170% the modeled streamflow becomes more and more accurate (NSCE becomes closer to 1); however, increasing the spread beyond the value 170% results in no further improvement in the NSCE values.

For experiments 2 and 3, similar sensitivity tests were conducted and are shown in Fig. 5(b) and (c). Regarding the observation error, since the remotely-sensed AMSR-E signal converted streamflow shows an overestimate during the low-flow, dry seasons (Fig. 4), a relatively larger observation error of 10% (compared to ground gauge-based streamflow observation error of 8% in experiment 1) is assumed. These results are shown for experiments 2 and 3 in Fig. 6(b) and (c) respectively, both of which assimilate the AMSR-E observations. The optimal ensemble size for experiment 2 and 3 is the same as experiment 1. When fixing the ensemble size to 50 members, the simulated discharge skill reaches maximum values when the spread of precipitation approaches around 140% for both experiment 2 and experiment 3.

Of all the three factors potentially impacting data assimilation efficiency, ensemble size was the least sensitive while the spread of precipitation was the most sensitive. The sensitivity analysis shows that the error in the remotely-sensed precipitation estimates was around 140% to 170%. As mentioned in the introduction, studies show that the TRMM RT precipitation product can lead to bias and random errors that propagate into hydrologic modeling outputs. For hydrological forecasting, the error usually comes from a combination of uncertainties in the input data (TRMM RT and PET in this study), the model structure, and the initial conditions. In this study, the model structural errors were not quantified so that the inability of the model to generate accurate streamflow was translated into the input forcing data uncertainty. In other words, a larger spread of precipitation

is selected in this study to compensate for the modeling error in this case.

B. Calibration Analysis

As shown in Fig. 6, model calibration results are quite similar to one another, even when the gauge streamflow observation (experiment 1 & 2) or AMSR-E signal converted streamflow (experiment 3) was applied for calibration. When model parameters are adjusted using gauge-observed streamflow (experiments 1 and 2), the value of Bias, RMSE and NSCE are -11.08%, 68.33% and 0.61, respectively. When the model parameters are adjusted using the AMSR-E signal converted streamflow (experiment 3), the value of Bias, RMSE and NSCE are -8.11%, 75.78% and 0.61, respectively. The striking similarity of the calibration results using different streamflow data sources is a result of high consistency between the signal-converted streamflow and the gauge-observed streamflow. As shown in Fig. 4, the signal-converted streamflow matches quite well with the gauge observation especially during high flow periods. Moreover, the statistic used to compare the simulations and observations, NSCE, is much more sensitive to high flows compared to low flows. However, it is noted that because of the insensitivity of the AMSR-E sensor to low flows, there is significant overestimation of the signal-converted streamflow for dry periods. The apparent capability to use the AMSR-E signal to calibrate a hydrologic model while achieving nearly the same degree of high skill as using in-situ gauge observations highlights its great potential to be used in tandem with remotely-sensed precipitation data and PET for providing real-time flood detection and forecasts in sparsely gauged or ungauged basins.

C. Impact of Data Assimilation

1) Impact of Data Assimilation During Calibration Period: EnSRF is used to assimilate different sources of streamflow observations into the hydrological model and to estimate all the internal states, thus potentially improving the model outputs of discharge. In order to make the results comparable among those three experiments, the same ensemble size (50) and spread of precipitation (150%) were assumed during the implementation of the assimilation procedures into HyMOD. Since the observation error of the AMSR-E signal converted streamflow shows significant overestimation during low flows, a larger observation error of 10% (in experiment 2 & 3) was assumed while 8% was assumed with the gauge observation error (in experiment 1). The precipitation forcing was perturbed by adding Gaussian white noise through multiplying the TRMM RT daily data by a multiplier of which the mean is 1.0 and the standard deviation is 150%. If negative values appear during the random multiplier generating, the code will automatically re-conduct the Gaussian distributed multiplier generation until they are all positive values.

Overall, Fig. 6 shows the streamflow "Open Loop" ensembles (grey lines), data "Assimilation" ensembles (yellow lines), Open Loop Ensemble Mean (green dash line), Assimilation Ensemble Mean (red dash line), Open Loop deterministic model run (blue dash line), gauge observation (dark solid line), and signal converted streamflow (magenta dash-dot line). Compared to streamflow ensembles before data assimilation (grey lines), the streamflow ensemble spread after data assimilation (yellow lines) is much reduced, and the ensemble mean after the assimilation is also much closer to the observations. This result reflects the effectiveness of the EnSRF. Compared with the deterministic Open Loop run, which is the modeled streamflow driven by the original TRMM RT precipitation data without perturbation, the Open Loop ensemble mean is overestimated due to the discard of negative values during the precipitation perturbation procedure as mentioned in the end of last paragraph.

For the assimilation module, the statistical evaluation excludes the first three month for both calibration and validation period due to the bad first guesses at the beginning of each period; in order to make a "fair" comparison between Open-Loop and Assimilation, for Open Loop module, statistics were also calculated excluding the first three months of each period. Experiment 1 is the benchmark for the experiments as it represents a traditional calibration using rainfall and gauged runoff observations while including a streamflow data assimilation step. Fig. 6(a) shows the impact of the assimilation procedure on the modeled streamflow in the benchmark experiment 1. By assimilating the gauge-based streamflow observation into the gauge-calibrated HyMOD, the Bias is improved from -11.08% to -1.39%, RMSE reduces from 68.33% to 29.50%, while NSCE goes up from 0.61 to 0.91. These statistical results all indicate significant improvement in the modeled streamflow following the assimilation of gauge-based streamflow during the calibration period from 2003 to 2005.

In the second and third experiments, the effectiveness of assimilating AMSR-E signal converted streamflow into HyMOD, conditioned on calibrations from different streamflow sources was assessed. In the second experiment, the model was calibrated by gauge streamflow and then the AMSR-E signal converted to streamflow was assimilated into HyMOD. In the third experiment, the AMSR-E signal converted to streamflow was used as the source for both model calibration and assimilation. Similar results were obtained in experiments 2 and 3 compared to the first experiment. Specifically, after the EnSRF data assimilation technique was applied, values of RMSE dropped while NSCE rose. This justifies its use for improving discharge simulations.

Furthermore, in order to further evaluate the potential advantage of using data assimilation approach, ensemble spread before (blue solid line) and after (red solid line) data assimilation and the absolute error between modeled streamflow and observed streamflow for both Open Loop module (blue dotted line) and Assimilation module (red dotted line) were plotted in Fig. 7. As expected, the ensemble spread is greatly reduced using the EnSRF relative to the Open-Loop, and the absolute error is also reduced after applying the EnSRF compared to the Open-Loop, especially during the validation period.

2) Impact of Data Assimilation During Validation Period: During the validation period from 2006 to 2007, the modeling performance without streamflow assimilation has deteriorated at a significant level compared to the calibration period in terms of Bias, RMSE and NSCE in all three experiments as shown in the tables located in the lower panels in Fig. 6(a), (b), and (c), respectively. Both the simplicity of the model structure and the

inter-annual uncertainties in the remotely-sensed TRMM RT precipitation contribute to this deterioration.

However, the application of EnSRF to assimilate different sources of streamflow observation improves the 1-day streamflow prediction. All the experiments' modeling results have been remarkably enhanced for the "Assimilation" component compared to the "Open Loop" during the validation period. In comparing the statistics in the three experiments, experiment 2 reveals a slight degradation in all three scores in comparison to the benchmark in the first experiment. Nonetheless, the degradation isn't significant indicating the potential application of assimilating the AMSR-E signal even into a hydrologic model that has been previously calibrated from gauge observations. As expected, the best statistical results were associated to experiment 1. Experiment 3, which was based on calibration and assimilation using the AMSR-E signal alone, outperformed experiment 2 and has competitive results to experiment 1 as well. The comparable modeling performance of experiment 3 compared to experiment 1 clearly highlights the potential of using the remote-sensing data as a proxy for streamflow with application for flood early warning in sparsely-gauged or ungauged basins. The above results demonstrate that even using a simple hydrological model, when coupled with the EnSRF data assimilation approach, together with large perturbations of precipitation to compensate for the model structural deficiencies, a satisfactory modeling performance can be produced for streamflow forecasting. Further evaluations based on extreme events are conducted in the next section.

D. Threshold-Based Evaluation and Analysis

As shown in Fig. 8, a threshold for high flow is calculated by ranking the daily streamflow data from 1946 to 2005 (50 years) at the Rundu gauge station from highest to lowest. The discharge corresponding to the top 10% daily streamflow quantile, with a value of 402 m^3/s, is identified as the high flow threshold.

POD, FAR, CSI and ETS were calculated to further evaluate the filter's performance focused on the detection-capability of the top 10% daily streamflow quantile for the three experiments as before. Fig. 9 indicates that after data assimilation, POD, CSI and ETS increase while FAR decreases for all experiments during both calibration (left panel in Fig. 9) and validation (right panel in Fig. 9) period experiments except for the POD in the validation period. The POD values without data assimilation are equal to one for the reason that the modeled streamflow is significantly overestimated during the validation period (as shown in Fig. 6) with all "hits" and no "misses". Nonetheless, the major improvements of POD, FAR, CSI and ETS during both the calibration and validation period highlight the efficiency of high flow detection following data assimilation. These categorical verification statistics together with Bias, RMSE, and NSCE indicate that the impact of the data assimilation procedure to the modeled streamflow is beneficial, especially for improving the model simulation skill during flood events mainly due to the fact that the AMSR-E sensor is quite sensitive to high flow events. During these flooding cases the difference between the brightness temperature for the calibration pixel and the measurement pixel is more acute due to the expansion of the river's surface area.

For experiment 3, which fully depends on the remote-sensing inputs and highlights the potential of flood prediction in ungauged basins, POD, CSI, and ETS showed improvements after implementing the data assimilation approach during the high flow period. Compared with experiment 1 during the calibration period, all the categorical verification statistics show improvements to POD, FAR, CSI, and ETS following data assimilation. When it comes to the validation period, the flood detection capability of experiment 3 is better than experiment 2, but slightly degraded yet comparable to experiment 1, which indicates the AMSR-E signal converted to streamflow was apparently well adapted to the model. These experiments highlight the potential use of the AMSR-E signal for streamflow prediction during flooding seasons, especially in ungauged basins.

V. Conclusion

Though data scarcity remains a big challenge in hydrologic modeling, remote-sensing data provide a promising perspective on advancements in this research area. In addition, data assimilation techniques incorporate the uncertainties from both the input data and initial conditions and also have the potential to enhance modeling performance. In this study, the deterministic Ensemble Kalman Filter – Ensemble Square Root Filter was coupled with a widely used conceptual rainfall-runoff model to assimilate streamflow data from either in-situ or remote sensing sources to update all the internal states in the model, thus providing the potential to improve modeling results. The following conclusions are reached in this study:

(1) AMSR-E brightness temperature signals can be successfully used to estimate streamflow, highly consistent with the in-situ observation. In particular, the signal converted to streamflow matches well with the observation over relatively high flow periods due to its high sensitivity to land surface wetness.

(2) The traditional model calibration technique is subject to uncertainties in the data, parameters, internal states and model structure. The general poor performance of the calibrated model can be attributed to the weakness of traditional calibration techniques that are normally constrained or limited from the inaccuracy of input remote sensing precipitation data and the simplification of the model structure. Data assimilation can account for both the uncertainties in the input data and the model structure by updating the internal model states, so it is a promising tool in improving hydrological modeling performance, especially for applications of real-time forecasts for decision-makers.

(3) The modeling results have been found to be insensitive to the ensemble size since the model used is a lumped model and there are only a total of five internal states in this conceptual rainfall-runoff model. In contrast, the spread of the precipitation is more sensitive to the improvements of the modeled streamflow.

(4) The three experiments show that through the assimilation of either the gauged streamflow or the AMSR-E signal converted to streamflow into the hydrological model by EnSRF, the difference between the streamflow simulation and observation can be reduced. This

demonstrates that EnSRF is effective and efficient in improving modeling performance by assimilating different sources of high-quality streamflow data. The first experiment is the benchmark to verify the feasibility and effectiveness of the data assimilation approach. The second experiment proves the modeling improvement via assimilating a different source of streamflow (i.e., satellite-based streamflow) into a hydrological model that was calibrated by the in-situ streamflow observations. In the third experiment, the AMSR-E streamflow signals were used first to calibrate the model and then assimilated into the model without in-situ streamflow data, thus demonstrating the potential usefulness of the AMSR-E signal data to benchmark and improve hydrological predictions in ungauged or undergauged basins.

(5) When taking the corresponding value to the upper 10th percentile of daily streamflow observations for the recent 50 years as the high flow threshold, the assimilation of both gauge-based streamflow and AMSR-E signal converted to streamflow into HyMOD not only increases POD, CSI, and ETS but also decreases FAR, thus further improving the modeling results for flood forecasting in the Cubango river basin.

(6) Previous studies on hydrological data assimilation commonly take the traditional observation as assimilation data sources, i.e., gauge-observed soil moisture [22], [26] and observed streamflow [22], [27], [28]. Benefitting from remote-sensing techniques, recent studies incorporated remotely sensed soil moisture as assimilation sources to improve the discharge prediction [21], [23]–[25]. So far, no remotely sensed streamflow information has been applied for hydrological data assimilation. As mentioned in [42], currently, river discharge cannot be directly measured by satellite sensors. However, passive microwave sensors – AMSR-E together with TRMM TMI have been used to detect river discharge changes, and those information can be converted into streamflow by using the algorithm mentioned in [31]. This study is the "first attempt" to exploit and demonstrate the applicability of assimilating spaceborne passive microwave streamflow signals to improve flood prediction in the sparsely gauged Cubango River basin in Africa. Compared to the closest previous publication Khan *et al.* [50] which has also investigated the applicability of the AMSR-E signals in hydrological modeling in the same research region, this study used a simple yet robust model and conducted competitive results. A data assimilation technique is used in this study in addition to the traditional calibration compared to Khan *et al.* [50]. Ensemble streamflow simulations are generated and then the ensemble mean is calculated as the final output to represent the streamflow simulation; When combined with EnSRF data assimilation approach HyMOD has similar results compared to a complex, distributed CREST hydrologic model.

In closing, this study is the "first attempt" to exploit and demonstrate the applicability of assimilating spaceborne AMSR-E streamflow signals to improve flood prediction in the Cubango River basin. It also shows that opportunities and challenges exist for an integrated application of a suite of satellite data to flood prediction by careful fusion of remote sensing and in-situ observations and further effective assimilation of the information into a hydrological model. Given the global availability of satellite-based precipitation and AMSR-E signal information in near real-time, we argue that this work will also contribute to the decadal initiative of Prediction in Ungauged Basins: a paradigm shift in the streamflow prediction methods away from traditional methods reliant on statistical analysis and calibrated models, and towards new techniques and new kind of observations, particularly imperative for the vast ungauged or undergauged basins around the world. More promising, data assimilation of remote sensing information for improving hydrological prediction can be increasingly appreciated and supported by the current TRMM and future GPM (Global Precipitation Mission, to be launched in July 2013) together with the current Aqua/AMSR-E and future SMAP (Soil Moisture Active and Passive, to be launched in 2014). Both the new missions are anticipated to provide better precipitation and soil moisture data in terms of coverage, accuracy, and resolutions.

APPENDIX

Table III shows the contingency table for streamflow simulation and ground gauge observation comparisons. For the case that both the streamflow simulation and ground gauge observation are higher than a certain threshold, it is "hit"; for the case that the streamflow simulation is lower than the certain threshold when ground gauge observation is higher than the same threshold, it is "miss"; for the case that the streamflow simulation is higher than the certain threshold but mean while ground gauge observation is lower than the same threshold, it is "false alarm"; for the case that both the streamflow simulation and ground gauge observation are lower than the certain threshold, it is "Correct Rejection". The desirable values for POD, FAR, CSI and ETS are 1, 0, 1 and 1, respectively.

Probability of Detection measures the fraction of observed events that exceeded the top 10% daily streamflow quantile that were correctly simulated:

$$POD = \frac{hit}{hit + miss}. \tag{A1}$$

False Alarm Ratio calculates the fraction of simulated events that exceeded the top 10% daily streamflow quantile that were not observed:

$$FAR = \frac{false\ alarm}{hit + false\ alarm}. \tag{A2}$$

The Critical Success Index, which is also called Threat score, gives the overall fraction of correctly detected events that exceeded the top 10% daily streamflow quantile:

$$CSI = \frac{hit}{hit + miss + false\ alarm}. \tag{A3}$$

The Equitable Threat Score, which describes how well the simulated "yes" events are corresponding to the observed "yes" events that exceeded the top 10% daily streamflow quantile:

$$ETS = \frac{Hits - E}{Hits + Miss + False\ Alarm}$$
$$E = \frac{\#Forecast\ points \times \#Observed\ points}{\#\ of\ Total\ points\ possible}. \quad \text{(A4)}$$

ACKNOWLEDGMENT

The authors would like to gratefully acknowledge the Global Flood Detection System for providing the AMSR-E M/C ratio signal data to conduct this study.

REFERENCES

[1] Z. Kugler and T. D. Groeve, The Flood Detection System, JRC Scientific and Technical Reports, EUR 23303 EN – 2007.

[2] Y. Hong, R. F. Adler, A. Negri, and G. J. Huffman, "Flood and landslide applications of near real-time satellite rainfall estimation," *J. Natural Hazards*, vol. 43, no. 2, 2007.

[3] P. Adhikari, Y. Hong, K. R. Douglas, D. Kirschbaum, J. J. Gourley, R. F. Adler, and G. R. Brakenridge, "A digitized global flood inventory (1998–2008): Compilation and preliminary results," *J. Natural Hazards*, vol. 55, pp. 405–422, 2010.

[4] J. McCarthy, *Climate Change 2001: Impacts, Adaptation, and Vulnerability: Contribution of Working Group II to the Third Assessment Report of the Intergovernmental Panel on Climate Change*. Cambridge, U.K.: Cambridge University Press, 2001.

[5] V. Kuzmin, D. J. Seo, and V. Koren, "Fast and efficient optimization of hydrologic model parameters using a priori estimates and stepwise line search," *J. Hydrology*, vol. 353, pp. 109–128, 2008.

[6] Q. Duan, S. Sorooshian, and V. K. Gupta, "Optimal use of the SCE-UA global optimization method for calibrating watershed medels," *J. Hydrology*, vol. 158, pp. 265–284, 1994.

[7] J. A. Vrugt, C. J. F. ter Braak, C. G. H. Diks, B. A. Robinson, J. M. Hyman, and D. Higdon, "Accelerating Markov chain Monte Carlo simulation by different evolution with self-adaptive randomized subspace sampling," *Int. J. Nonlinear Sci. Numer. Simulation*, vol. 10, no. 3, pp. 1–12, 2009.

[8] A. R. Robinson, P. F. J. Lermusiaux, and N. Q. Sloan, III, "Data assimilation," in *"The Sea: The Global Coastal Ocean I", Processes and Methods*, K. H. Brink and A. R. Robinson, Eds. New York, NY, USA: Wiley, 1998, vol. 10, pp. 541–594.

[9] R. H. Reichle, D. B. McLaughlin, and D. Entekhabi, "Hydrologic data assimilation with the ensemble Kalman filter," *Monthly Weather Rev.*, vol. 130, pp. 103–114, 2002.

[10] "Panel on model-assimilated data sets for atmospheric and oceanic research," in *Four-Dimensional Model Assimilation of Data: A Strategy for the Earth System Sciences*. Washington, DC, USA: National Academy Press, 1991, p. 78.

[11] P. L. Houtekamer and H. L. Mitchell, "A sequential ensemble Kalman filter for atmospheric data assimilation," *Monthly Weather Rev.*, vol. 129, pp. 123–37, 2001.

[12] P. L. Houtekamer and H. L. Mitchell, "Reply to comment on "Data assimilation using an ensemble Kalman filter technique"," *Monthly Weather Rev.*, vol. 127, pp. 1378–9, 1999.

[13] P. L. Houtekamer and H. L. Mitchell, "Data assimilation using an ensemble Kalman filter technique," *Monthly Weather Rev.*, vol. 126, pp. 796–811, 1998.

[14] T. M. Hamill, J. S. Whitaker, and C. Snyder, "Distance-dependent filtering of background-error covariance estimates in an ensemble Kalman filter," *Monthly Weather Rev.*, vol. 129, pp. 2776–90, 2001.

[15] H. L. Mitchell, P. L. Houtekamer, and G. Pellerin, "Ensemble size, balance, and model-error representation in an ensemble Kalman filter," *Monthly Weather Rev.*, vol. 130, pp. 2791–808, 2002.

[16] J. L. Anderson, B. Wyman, S. Zhang, and T. Hoar, "Assimilation of surface pressure observations using an ensemble filter in an idealized global atmospheric prediction system," *J. Atmospheric Sciences*, vol. 62, pp. 2925–2938, 2005.

[17] A. Caya, J. Sun, and C. A. Snyder, "A comparison between the 4D-VAR and the ensemble Kalman filter techniques for radar data assimilation," *Monthly Weather Rev.*, vol. 133, pp. 3081–3094, 2005.

[18] X. Wang, C. Snyder, and T. M. Hamill, "On the theoretical equivalence of differently proposed ensemble–3DVAR hybrid analysis schemes," *Monthly Weather Rev.*, vol. 135, pp. 222–227, 2007.

[19] X. Wang, T. M. Hamill, J. S. Whitaker, and C. H. Bishop, "A comparison of the hybrid and EnSRF analysis schemes in the presence of model errors due to unresolved scales," *Monthly Weather Rev.*, vol. 137, pp. 3219–3232, 2009.

[20] D. C. Dowell, L. J. Wicker, and C. Snyder, "Ensemble Kalman filter assimilation of radar observations of the 8 May 2003 Oklahoma City supercell: Influences of reflectivity observations on storm-scale analyses," *Monthly Weather Rev.*, vol. 139, pp. 272–294, 2011.

[21] R. N. Pauwels, R. Hoeben, N. E. Verhoest, F. P. De Troch, and P. A. Troch, "Improvements of TOPLATS-based discharge predictions through assimilation of ERS-based remotely-sensed soil moisture values," *Hydrological Process*, vol. 16, pp. 995–1013, 2002.

[22] D. Aubert, C. Lourmagne, and L. Oudin, "Sequential assimilation of soil moisture and streamflow data in a conceptual rainfall-runoff model," *J. Hydrology*, vol. 280, pp. 145–161, 2003.

[23] W. T. Crow, R. Bindlish, and T. J. Jackson, "The added value of spaceborne passcive microwave soil moisture retrievals for forecasting rainfall-runoff ratio partitioning," *Geophysical Res. Lett.*, vol. 32, p. L18401, 2005.

[24] W. T. Crow and D. Ryu, "A new data assimilation approach for improving runoff prediction using remotely-sensed soil moisture retrievals," *Hydrology and Earth Syst. Sciences*, vol. 13, pp. 1–16, 2009.

[25] H. Gao, E. F. Wood, M. Drusch, and M. F. McCabe, "Copula-derived observation operators for assimilating TMI and AMSR-E retrieved soil moisture into land surface models," *J. Hydrometeorology*, vol. 8, pp. 413–429, 2007.

[26] F. Chen, W. T. Crow, P. J. Starks, and D. N. Moriasi, "Improving hydrologic predictions of a catchment model via assimilation of surface soil moisture," *Advances in Water Resources*, vol. 34, pp. 526–536, 2011.

[27] R. N. Pauwels and G. J. M. De Lannoy, "Improvement of modeled soil wetness conditions and turbulent fluxes through the assimilation of observed discharge," *J. Hydrometeorology*, vol. 7, pp. 458–477, 2006.

[28] M. P. Clark, D. E. Rupp, R. A. Woods, X. Zheng, R. P. Ibbitt, A. G. Slatter, J. Schmidt, and M. J. Uddsrom, "Hydrological data assimilation with the ensemble Kalman filter: Use of streamflow observations to update states in a distributed hydrological model," *Advances in Water Resources*, vol. 31, pp. 1309–1324, 2008.

[29] L. C. Smith, "Satellite remote sensing of river inundation area, stage, and discharge: A review," *Hydrological Process*, vol. 11, no. 10, pp. 1427–1439, 1997.

[30] G. R. Brakenridge, E. Anderson, S. V. Nghiem, S. Caquard, and T. B. Shabaneh, "Flood warnings, flood disaster assessments, and flood hazard reduction: The roles of orbital remote sensing," in *30th Int. Symp. Remote Sensing of Environment*, Honolulu, HI, USA, Nov. 10–14, 2003.

[31] G. R. Brakenridge, S. V. Nghiem, E. Anderson, and R. Mic, "Orbital microwave measurement of river discharge and ice status," *Water Resources Res.*, vol. 43, no. 4, p. W04 405, 2007.

[32] J. J. Gourley, Y. Hong, Z. L. Flamig, J. Wang, H. Vergara, and E.N. Anagnostou, "Hydrologic evaluation of rainfall estimates from radar, satellite, gauge, and combinations on Ft. Cobb basin, Oklahoma," *J. Hydrometeorology*, 2011.

[33] M. M. Bitew and M. Gebremichael, "Evaluation of satellite rainfall products through hydrologic simulation in a fully distributed hydrologic model," *Water Resources Res.*, vol. 47, p. W06526, 2011.

[34] H. Moradkhani, S. Sorooshian, H. V. Gupta, and P. R. Houser, "Dual state-parameter estimation of hydrological models using ensemble Kalman filter," *Advances in Water Resources*, vol. 28, no. 2, pp. 135–147, 2005.

[35] C. Milzow, L. Kgotlhang, P. Bauer-Gottwein, P. Meier, and W. Kinzelbach, "Regional review: The hydrology of the Okavango Delta, Botswana—Processes, data and modeling," *Hydrogeology J.*, vol. 17, pp. 1297–1328, 2009.

[36] D. A. Hughes, L. Andersson, J. Wilk, and H. H. G. Savenije, "Regional calibration of the Pitman model for the Okavango River," *J. Hydrology*, vol. 331, pp. 30–42, 2006.

[37] C. Milzow, L. Kgotlhang, W. Kinzelbach, P. Meier, and P. Bauer-Gottwein, "The role of remote sensing in hydrological modelling of the Okavango Delta, Botswana," *J. Environmental Manage.*, vol. 90, pp. 2252–2260, 2009.

[38] J. M. McCarthy, T. Gumbricht, T. McCarthy, P. Frost, K. Wessels, and F. Seidel, "Flooding patterns of the Okavango Wetland in Botswana between 1972 and 2000," *AMBIO: A J. Human Environment*, vol. 32, no. 7, pp. 453–457, 2003.

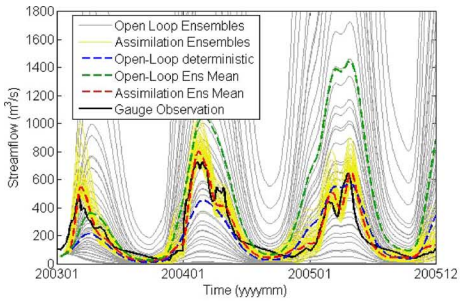

(a1)

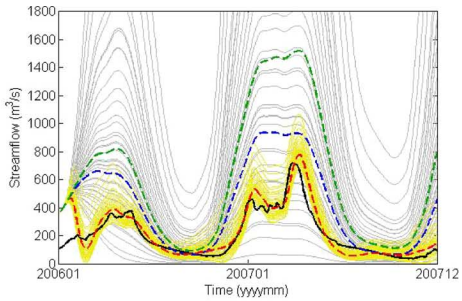

(a2)

exp1	Calibration			Validation		
	Bias(%)	RMSE(%)	NSCE	Bias(%)	RMSE(%)	NSCE
Open Loop	-11.08	68.33	0.61	104.25	140.62	-2.01
Assimilation	-1.39	29.50	0.91	-7.02	34.59	0.92

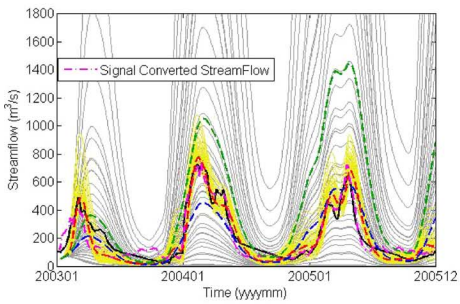

(b1)

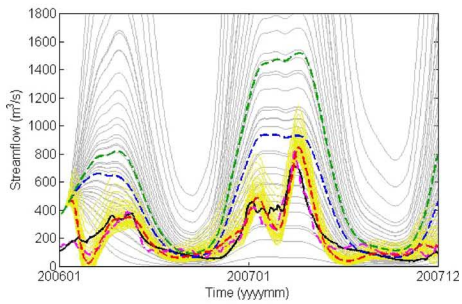

(b2)

exp2	Calibration			Validation		
	Bias(%)	RMSE(%)	NSCE	Bias(%)	RMSE(%)	NSCE
Open Loop	-11.08	68.33	0.61	104.25	140.62	-2.01
Assimilation	2.65	37.27	0.87	-4.93	62.43	0.85

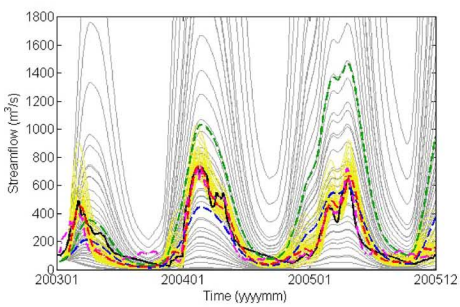

(c1)

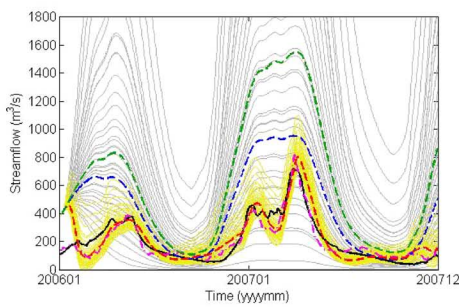

(c2)

exp3	Calibration			Validation		
	Bias(%)	RMSE(%)	NSCE	Bias(%)	RMSE(%)	NSCE
Open Loop	-8.11	75.78	0.61	109.90	161.43	-2.18
Assimilation	1.37	33.02	0.89	-7.21	36.88	0.87

Fig. 6. Comparisons between streamflows predictions before (open loop) and after (assimilation) data assimilation. (a) Experiment 1: model was calibrated by gauge streamflow and the data that used to be assimilated into the model was also gauge streamflow: (a1) for calibration period and (a2) for validation period. (b) Experiment 2: model was calibrated by gauge streamflow and the data that used to be assimilated into the model was the AMSR-E signal converted streamflow: (b1) for calibration period and (b2) for validation period. (c) Experiment 3: model was calibrated by AMSR-E signal converted streamflow and the data that used to be assimilated into the model was also the AMSR-E signal conversion: (c1) for calibration period and (c2) for validation period.

[39] L. Andersson, J. Wilk, M. C. Todd, D. A. Hughes, A. Earle, D. Kniveton, R. Layberry, and H. G. Savenije, "Impact of climate change and development scenarios on flow patterns in the Okavango River," *J. Hydrology*, vol. 331, pp. 43–57, 2006.

[40] D. A. Hughes, D. G. Kingston, and M. C. Todd, "Uncertainty in water resources availability in the Okavango River basin as a result of climate change," *Hydrology and Earth Syst. Sciences*, vol. 15, pp. 931–941, 2011.

[41] Q. Duan, S. Sorooshian, and V. K. Gupta, "Optimal use of the SCE-UA global optimization method for calibrating watershed models," *J. Hydrology*, vol. 158, no. 3–4, pp. 265–284, 1994.

[42] T. Waneger, D. P. Boyle, M. J. Lees, H. S. Wheater, H. V. Gupta, and S. Sorooshian, "A framework of development and application of hydrological models," *Hydrol. Earth Syst. Sci.*, vol. 5, no. 1, pp. 13–26, 2001.

[43] R. S. Blasone, J. A. Vrugt, H. Madsen, D. Rosbjerg, B. A. Robinson, and G. A. Zyvoloski, "Generalized likelihood uncertainty estimation 885 (GLUE) using adaptive Markov Chain Monte Carlo sampling," *Advances in Water Resources*, vol. 31, pp. 630–648, 2008.
[44] J. B. Kollat, P. M. Reed, and T. Wagener, "When are multiobjective calibration trade-offs in hydrological models meaningful?," *Water Resources Res.*, vol. 48, p. W03520, 2012.
[45] C. Milzow, P. E. Krogh, and P. Bauer-Gottwein, "Combining satellite radar altimetry, SAR surface soil moisture and GRACE total storage changes for model calibration and validation in a large ungauged catchment," *Hydrol. Earth Syst. Sci.*, vol. 15, pp. 1729–1743, 2011.
[46] G. J. Huffman, D. T. Bolvin, E. J. Nelkin, D. B. Wolff, R. F. Adler, G. Gu, Y. Hong, K. P. Bowman, and E. F. Stocker, "The TRMM Multisatellite Precipitation Analysis (TMPA): Quasi-global, multiyear, combined-sensor precipitation estimates at fine scales," *J. Hydrometeorology*, vol. 8, pp. 38–55, 2007.
[47] M. Temimi, T. Lacava, T. Lakhankar, V. Tramutoli, H. Ghedira, R. Ata, and R. Khanbilvardi, "A multi-temporal analysis of AMSR-E data for flood and discharge monitoring during the 2008 flood in Iowa," *Hydrological Processes*, vol. 25, no. 16, pp. 2623–2534, 2011.
[48] M. Temimi, R. Leconte, F. Brissette, and N. Chaouch, "Flood and soil wetness monitoring over the Mackenzie River Basin using AMSR-E 37 GHz brightness temperature," *J. Hydrology*, vol. 333, no. 2, pp. 317–328, 2007.
[49] M. Salvia, F. Grings, P. Ferrazzoli, V. Barraza, V. Douna, P. Perna, and H. Karszenbaum, "Estimating flooded area and mean water level using active and passive microwaves: The example of Paraná River Delta floodplain," *Hydrol. Earth Syst. Sci.—Discussion*, vol. 8, pp. 2895–2928, 2011.
[50] S. I. Khan, Y. Hong, H. J. Vergara, J. J. Gourley, G. R. Brakenridge, T. De Groeve, Z. L. Flamig, F. Policelli, and B. Yong, "Microwave satellite data for hydrologic modeling in ungauged basins," *IEEE Geosci. Remote Sens. Lett.*, vol. 9, no. 4, pp. 663–667, Jul. 2012.
[51] J. S. Whitakey and T. M. Hamill, "Ensemble data assimilation without perturbed observations," *Monthly Weather Rev.*, vol. 7, no. 130, pp. 1913–1924, 2002.
[52] V. B. Sauer and R. W. Meyer, Determination of Error in Individual Discharge Measurements, U.S. Geological Survey, 1992, Open-File Report 92-144.

Yu Zhang is currently working toward the Ph.D. degree in the School of Civil Engineering and Environmental Science at the University of Oklahoma, Norman, OK, USA.

She is a research assistant in the HyDROS lab (Hydrometeorology and Remote Sensing Laboratory, http://hydro.ou.edu) and serves as Hydro Data Assimilation sub-group leader. Her research interests include hydrological data assimilation, global/regional hydrological forecasting, and application of remote sensing data in hydrology.

She is a student member of the American Geophysical Union.

Yang Hong received the B.S. and M.S. degrees in geosciences and environmental sciences from Peking University, Beijing, China, and the Ph.D. degree, major in hydrology and water resources and minor in remote sensing and spatial analysis, from the University of Arizona, Tucson, AZ, USA.

Following a postdoctoral appointment in the Center for Hydrometeorology and Remote Sensing, University of California, Irvine, CA, USA, he joined the National Aeronautics and Space Administration Goddard Space Flight Center, Greenbelt, MD, USA, in 2005. He is currently an Associate Professor with the School of Civil Engineering and Environmental Sciences and the School of Meteorology, University of Oklahoma, Norman, OK, USA, where he is also directing the Remote Sensing Hydrology research group (http://hydro.ou.edu). He also serves as the Co-director of the Water Technologies for Emerging Regions Center (http://water.ou.edu) and an affiliated Faculty Member with the Atmospheric Radar Research Center (http://arrc.ou.edu). He has served in the editorial boards of the International Journal of Remote Sensing, the Natural Hazards journal, and the Landslides journal. His primary research interests are in remote-sensing retrieval and validation, hydrology and water resources, natural hazard prediction, land surface modeling, and data assimilation systems for water resource planning under changing climate.

Dr. Hong is currently the American Geophysical Union Precipitation Committee Chair.

XuGuang Wang received the Ph.D. degree in Meteorology from the Pennsylvania State University, University Park, PA, USA.

She is currently an Assistant Professor in the School of Meteorology of University of Oklahoma, Norman, OK, USA. Her primary research interests lie in data assimilation and ensemble forecasting. Her research ranges from developing new theories and novel methodologies for data assimilation and ensemble forecasting, to specific applications on the predictions of atmospheric phenomena of various scales such as extra-tropical and tropical cyclones and severe convective storms, and to applying ensemble forecasting and data assimilation to understand the atmospheric predictability and dynamics.

Dr. Wang received the NASA New Investigator Award in 2010.

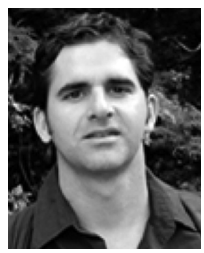

Jonathan J. Gourley received the B.S. and M.S. degrees in meteorology with a minor in hydrology and the Ph.D. degree in civil engineering and environmental science from the University of Oklahoma, Norman, OK, USA.

He is currently a Research Hydrometeorologist with NOAA's National Severe Storms Laboratory, is an affliate Associate Professor with the School of Meteorology, University of Oklahoma, and Director of the National Weather Center's seminar series. His research focuses on rainfall observations from remote sensing platforms with an emphasis on ground-based radars and implementing these high-resolution observations into hydrologic models. He completed a postdoctoral study with researchers in Paris, France, to demonstrate the capabilities of dual-polarimetric radar in improving data quality, microphysical retrievals, and precipitation estimation. MeteoFrance has subsequently upgraded several of their operational radars with polarimetric technology.

Dr. Gourley received the Department of Commerce Silver Medal Award in 1999 "For developing an important prototype Warning Decision Support System for weather forecasters and making significant enhancements to the NEXRAD system, resulting in more timely and reliable warnings." He also received an Honorable Mention in 2004 from the Universities Council on Water Resources Dissertation Awards Committee.

JiDong Gao received the B.S., M.S., and Ph.D. degrees from Lanzhou University, China, in 1988, 1991, and 1994, respectively.

He is currently a research meteorologist for National Severe Storm Laboratory (NSSL)/National Oceanic and Atmospheric Administration (NOAA), and adjunct associate professor of School of Meteorology/University of Oklahoma. His research focuses on variational atmospheric data assimilation (3DVAR/4DVAR), ensemble based data assimilation, and their applications to Doppler radar data quality control, single/multiple Doppler velocity retrieval, and assimilating radar data into high resolution Numerical Weather Prediction (NWP) models. He has authored and co-authored over 40 refereed journal articles and about 60 non-refereed conference publications in these research areas. Before joining NSSL/NOAA, he was a long time employee for Center for Analysis and Prediction of Storms, University of Oklahoma and generated over $1 million in external research grant as a Principal Investigator (PI) and over $3 million research grant as a Co-PI. He also devoted a lot of time into development of both 3DVAR/4DVAR system for the Advanced Regional Prediction System (ARPS), a nonhydrostatic mesoscale and storm scale NWP model.

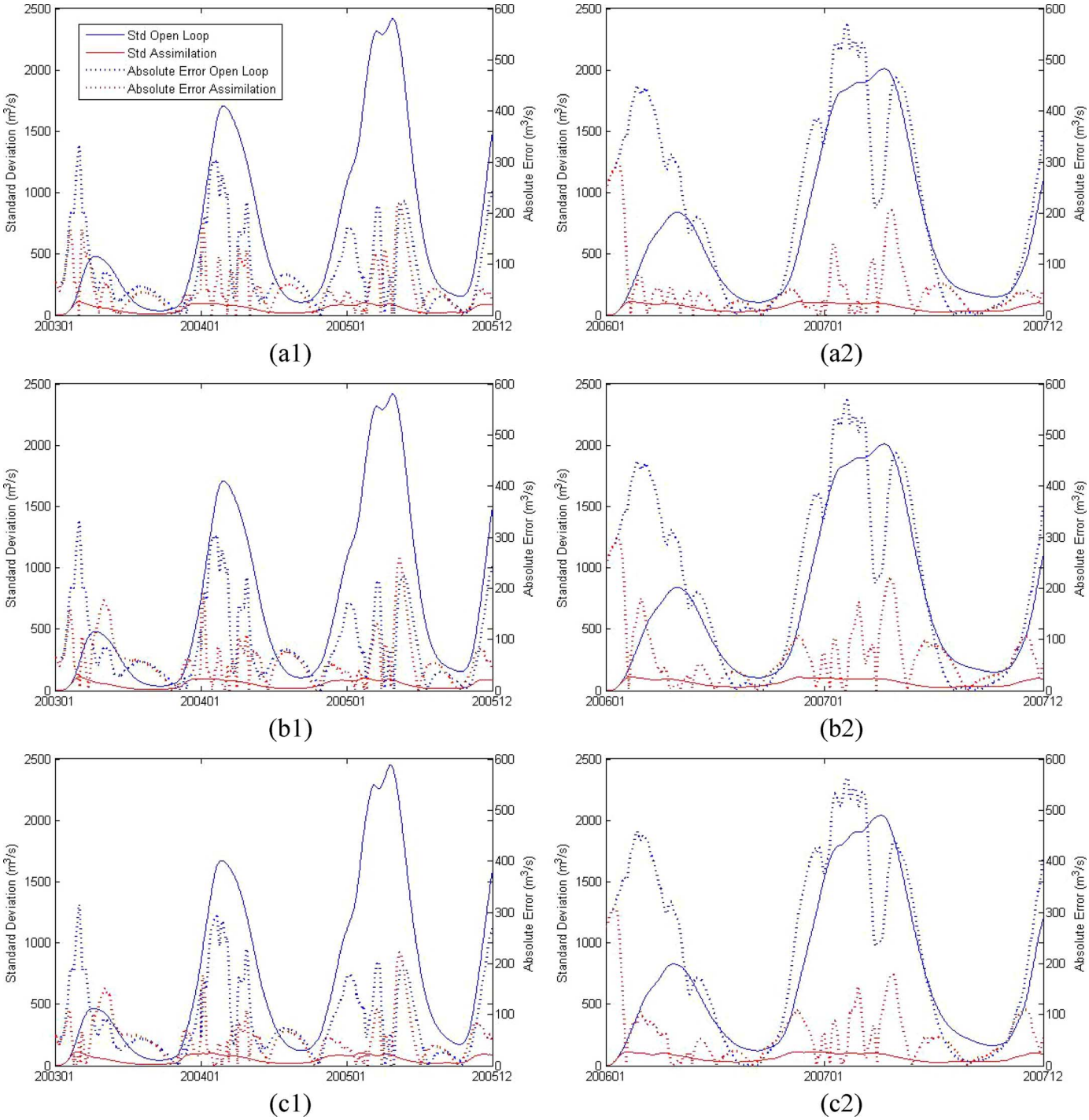

Fig. 7. Time series error analysis for Experiment 1 (Fig. 7(a)), Experiment 2 (Fig. 7(b)) and Experiment 3 (Fig. 7(c)). The left panels are corresponding to calibration period, the right panels are corresponding to validation period. The blue and red solid lines are the ensemble standard deviation for Open Loop module and Assimilation module respectively. The blue and red dash lines are the absolute error between the model simulated streamflow and the observed streamflow.

Humberto J. Vergara received the B.Sc. degree in environmental engineering from El Bosque University, Colombia, and the M.Sc. degree in water resources engineering from the University of Oklahoma, Norman, OK, USA. He is currently working toward the Ph.D. degree in the Department of Civil Engineering and Environmental Science at the University of Oklahoma, Norman.

He is currently a Graduate Research Assistant at the Hydrometeorology and Remote Sensing (HyDROS; hydro.ou.edu) Laboratory and the National Severe Storms Laboratory (NSSL; http://www.nssl.noaa.gov) in Norman, Oklahoma. His primary field of study is hydrological modeling for flood forecasting. He focuses on model development, ensemble forecasting and data assimilation.

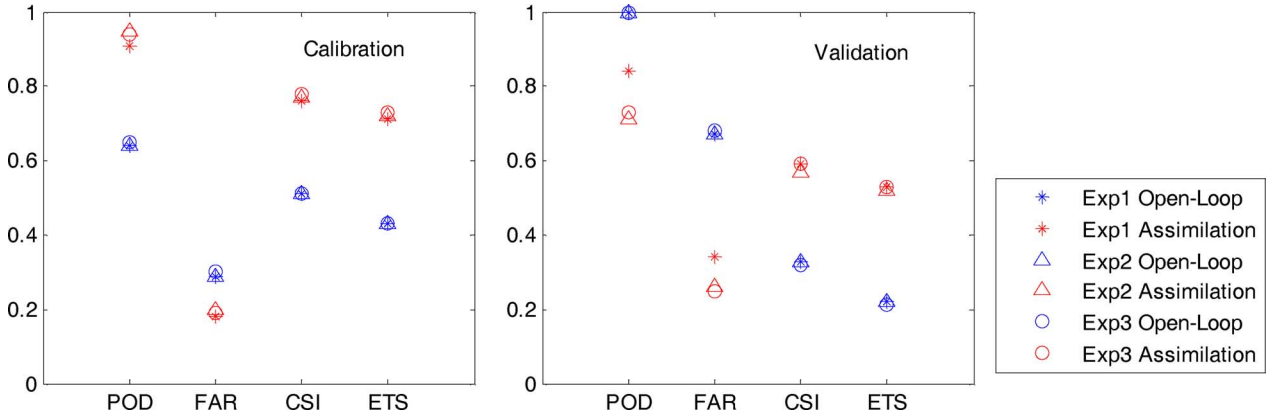

Fig. 9. Statistics (POD, FAR, CSI, ETS) plot during high flow.

TABLE III
CONTINGENCY SIMULATED STEAMFLOW (BEFORE AND AFTER) DATA ASSIMILATION APPLIED AND GROUND GAUGE OBSERVED STREAMFLOW.

		Ground Gauge Streamflow Observation	
		Yes	No
Simulate Streamflow Before/After DA	Yes	Hit	False Alarm
	No	Miss	Correct Rejection

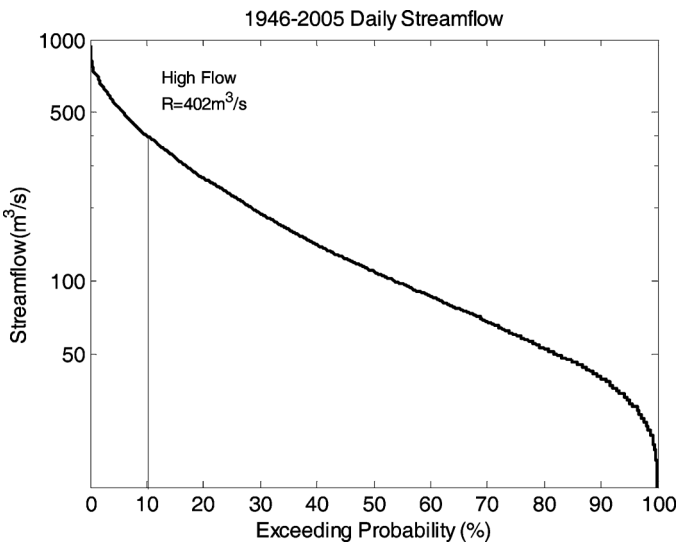

Fig. 8. Identification of high flow threshold.

Bin Yong received the B.S. degrees in Computer Science and Technology, Hefei University of Technology, Hefei, China, and the Ph.D. degree (successive master-doctor program) in cartography and geography information system from Nanjing University, Nanjing, China.

He is currently a Professor with the State Key Laboratory of Hydrology-Water Resources and Hydraulic Engineering, Hohai University, Nanjing, China. His research areas mainly includes: remote sensing precipitation (radar, satellite, multi-sensor, multi-platform); application of NASA multi-satellite products; and surface water and hydrological system analysis.

Dr. Yong is currently a member of the American Geophysical Union.